Journal of Sound and Vibration (1999) **224**(1), 69–99
Article No. jsvi.1999.2158, available online at http://www.idealibrary.com on IDEAL®

FSI ANALYSIS OF LIQUID-FILLED PIPES

L. ZHANG

Civil Engineering Department, *Yunnan Polytechnic University*, *Kunming* 650051, *Yunnan*, *People's Republic of China*

A. S. TIJSSELING AND A. E. VARDY

Civil Engineering Department, *University of Dundee*, *Dundee DD*1 4*HN*, *Scotland*

(*Received* 26 *July* 1996, *and in final form* 4 *January* 1999)

Most reported work on transient fluid/structure interaction (FSI) in liquid-filled pipes has been carried out in the time domain. When needed, information in the frequency domain (e.g., frequency responses) has been deduced by discrete Fourier transforms. In this paper, the analysis is undertaken directly in the frequency domain and has the advantage of enabling (linear) dispersive terms to be included in a fully coupled manner. In principle, time-domain results (e.g., pressure histories) can be obtained by numerical inverse Laplace transforms. In both domains, the mathematical model has one pair of equations for each mode of wave propagation—e.g., pressure waves in the liquid, flexural waves in the pipe. Axial FSI coupling exists in the equations and also in boundary conditions. The development used herein highlights common features between analysis in the frequency domain and analysis by the method of characteristics (MOC) in the time domain. A general formulation, not restricted to pipe systems, is presented. The method is validated by comparison with an alternative exact analytical solution, with results obtained by discrete Fourier transform from an MOC analysis and by comparison with measured data from a laboratory apparatus.

1. INTRODUCTION

Fluid/structure interaction (FSI) in liquid-filled pipe systems has been investigated extensively in the time domain [1, 2]. This can lead to a clear understanding of the underlying physical phenomena and it is a convenient way to explore the influence of arbitrarily varied boundary conditions. Suitable methods of numerical integration are widely practised and understood.

Notwithstanding this success, there are important practical advantages to be gained from considering the behaviour in the frequency domain, the most obvious being the prediction of natural frequencies. In principle, this information can be obtained from discrete Fourier transforms of time-domain results, but this is only partially effective. It does not, for instance, provide mode shapes for single frequency excitation (except through repeat analyses). Furthermore, the time-domain analysis must be undertaken in greater detail and

0022–460X/99/260069 + 31 $30.00/0

for longer simulation periods than is usually necessary for the simulation of transients. More important, the most popular time-domain analysis—the method of characteristics (MOC)—does not provide the frequency dependent wave speeds describing oscillatory flow phenomena.

The purpose of this paper is to present a method of analysis in the frequency domain that can be used with arbitrarily varied linear boundary conditions. The mathematical development is presented in a form that should be readily accessible to analysts more familiar with time domain analyses, especially MOC. Indeed, some of the key matrices are identical in the two cases.

1.1. FLUID/STRUCTURE INTERACTION (FSI)

Three coupling mechanisms determine FSI in straight pipes. *Friction coupling* is due to shear stresses resisting relative axial motion between the fluid and the pipe wall. These stresses act at the interface between the fluid and the pipe wall. *Poisson coupling* is due to normal stresses acting at this same interface. For example, an increase in fluid pressure causes an increase in pipe hoop stress and hence a change in axial wall stress. *Junction coupling* takes place at pipe boundaries that can move, either in response to changes in fluid pressure or because of external excitation.

1.2. PREVIOUS WORK

D'Souza and Oldenburger [3] Laplace transformed the variables, equations and boundary conditions describing the axial vibration of a liquid-filled pipe. Their model included unsteady laminar friction and junction coupling, but not Poisson coupling. It was validated by comparison with experimental data obtained from frequency response tests in a steel pipe filled with hydraulic oil.

Wilkinson [4] presented transfer matrices for the axial, lateral and torsional vibration of liquid-filled pipes. He included junction coupling, but not friction or Poisson coupling. Experimental results on a 1 m long, L-shaped, water-filled, steel pipe completed his work. The 70 mm bore pipes were excited by an external shaker.

El-Raheb [5] and Nanayakkara and Perreira [6] derived transfer matrices for straight and curved pipes, including the effects of junction coupling but excluding those of Poisson and friction coupling. The matrices formed the basis of a general algorithm to calculate the frequency response of, two-in reference [6] and three-in reference [5], dimensional unbranched pipe systems. Nanayakkara and Perreira compared their computational results on a single elbow pipe system with those obtained from three-dimensional finite element modelling and with experimental data from literature. Secondary acoustic loads resulting from non-planar wave effects due to bend curvature and straight-pipe imperfection were investigated theoretically by El-Raheb.

Kuiken [7] derived a transfer matrix for the axial vibration of a straight pipe including Poisson coupling, but not friction coupling. The effects of Poisson and junction coupling were studied in one numerical test case.

Lesmez [8, 9], Tentarelli [10, 11], Charley and Caignaert [12], De Jong [13, 14], Svingen and Kjeldsen [15] and Svingen [16, 17] applied the transfer matrix

method (TMM) to one-dimensional wave theory in the frequency response analysis of pipe systems. All incorporated Poisson and junction coupling in their theoretical models. Also, all presented experimental validation of their models—in some cases very impressively. The individual pipes were straight, but strong fluid/pipe and axial/lateral/torsional coupling between pipes occurred in some cases through the use of elbows and sections of curved pipe.

Lesmez [8, 9] performed experiments in a planar pipe system of variable length. The water-filled copper pipes had an inner diameter of 26 mm. A U-shaped test section with 1·8 m long legs was excited by an external shaker.

Tentarelli [10, 11] was the only one to include friction coupling. He allowed for axial pipe motion in the unsteady laminar friction model of D'Souza and Oldenburger [3]. He also presented a model for curved tubes. Five separate experiments on 10 mm inner diameter steel pipes filled with hydraulic oil were reported. Junction and Poisson coupling were investigated in a 1 m long straight pipe. Bourdon coupling, which occurs in curved pipes of non-circular cross-section, was predicted and observed in a J-shaped pipe. A planar 1·9 m long L-shaped system was used for the validation of two different elbow models. Finally, all FSI coupling mechanisms were combined in a three-dimensional system with three elbows, one curved section, one T-piece, two dead ends and one orifice. The pipes were excited by internal pressure excitation.

Charley and Caignaert [12] used experimental data obtained in a pump test rig to demonstrate that transfer matrices with FSI predict much better the measured pressure spectra than do the classical waterhammer [18, 19] transfer matrices, even in simple systems.

De Jong [13, 14] conducted experiments on a straight water-filled steel pipe (150 mm inner diameter, 1·5 m length) and on two such pipes connected by either an elbow or rubber bellows. Swept sine excitation of either liquid or pipes was used. A more comprehensive set-up was used in the experimental determination of the transfer matrix describing a centrifugal pump. Also, several models for curved tubes and elbows were compared.

Svingen's [15] TMM approach is based on the finite element method (FEM). His model includes frequency dependent damping. His laboratory apparatus [16, 17] consists of an L-shaped, water-filled, steel pipe placed in a vertical plane. The system is 20 m long and the 80 mm inner diameter pipes have 1 mm thin walls. The system is excited by a rotating disk, interrupting outflow to the open atmosphere. Gajić *et al.* [20] included linearized quasi-steady friction in a simulation of Svingen's experiment. More extensive literature reviews can be found in the quoted disserations [8, 10, 13, 17].

All of the above investigators applied harmonic excitations to their pipe systems. This is in contrast with the present paper, in which impact loads are considered. The immediate purpose is to use impact tests to determine natural frequencies and mode shapes. A more general aim is to move towards an analysis in the frequency domain yielding results that can be transformed numerically into the time domain for arbitrarily varied boundary conditions. For example, Adachi *et al.* [21] and Gopalakrishnan *et al.* [22] have followed this approach successfully. This will permit more reasonable representations of

frequency dependent phenomena than is possible in time-domain analyses. Possible applications of such analyses include unsteady friction, viscoelastic pipe wall materials and acoustic radiation in rock-bored tunnels [23–25].

1.3. OUTLINE OF PAPER

The general method of calculation is presented in section 2, particular emphasis being placed on features shared with the time-domain method of characteristics presented in Appendix A. In section 3, the analysis is applied to flexural vibrations of air-filled and water-filled pipes and is validated by comparison with the alternative analytical method of Huang [26] and with new experimental data. The more demanding case of axial vibrations is studied in section 4, in which comparisons are made with experimental measurements described in reference [27] and with discrete Fourier transforms of time-domain solutions. Section 5 contains the conclusions. A list of notation is given in Appendix D.

2. ANALYTICAL DEVELOPMENT

Suppose that the acoustic phenomenon under study can be represented in the time domain by the set of equations

$$\mathbf{A}(\partial/\partial t)\boldsymbol{\phi}(z, t) + \mathbf{B}(\partial/\partial z)\boldsymbol{\phi}(z, t) + \mathbf{C}\boldsymbol{\phi}(z, t) = \mathbf{r}(z, t), \tag{1}$$

where $\boldsymbol{\phi}$ denotes the vector of physical unknowns (velocity, pressure, etc.), and $\mathbf{A}$, $\mathbf{B}$ and $\mathbf{C}$ are matrices of constant coefficients. The vector $\mathbf{r}$ describes environmental sources of excitation. Both $\boldsymbol{\phi}$ and $\mathbf{r}$ represent *dynamic* (i.e., time-dependent) quantities, relative to the initial steady state (i.e., equilibrium) conditions. In general, there may be any even number of equations; in the particular applications considered in sections 3 and 4, there are four equations.

For all cases considered herein, the matrices $\mathbf{A}$ (or, more general, $\mathbf{A}^*$, defined later) and $\mathbf{B}$ are regular. The matrix $\mathbf{C}$, which contains terms causing dispersion, can be singular.

In the time domain, one of the most popular methods of analysis is the method of characteristics (MOC). It is used to find *ordinary* differential forms of equation (1) that are applicable in particular directions—such as wave paths ($\mathrm{d}z/\mathrm{d}t = c$, where c is a wave speed). This method is given in Appendix A.

An analogous approach is followed herein in the frequency domain. The Laplace transform of equation (1) can be treated as an ordinary differential equation and, in general, the solution can be found only for particular wave numbers $k = s/c$, where s is the Laplace parameter.

The Laplace transform of equation (1) is

$$s\mathbf{A}^*(s)\tilde{\boldsymbol{\phi}}(z, s) + \mathbf{B}(\partial/\partial z)\tilde{\boldsymbol{\phi}}(z, s) = \tilde{\mathbf{r}}(z, s) + \mathbf{A}\boldsymbol{\phi}(z, 0), \tag{2}$$

where the symbol $\sim$ denotes a transformed variable and the complex parameter s characterises the particular frequency under consideration. It is treated as a parameter in the analytical development. The matrix $\mathbf{A}^*$, introduced solely for clarity, is defined by

$$\mathbf{A}^*(s) = \mathbf{A} + (1/s)\mathbf{C}. \tag{3}$$

In the frequency domain, the matrices **A**, **B** and **C** may be complex—to represent frequency dependent parameters and damping mechanisms. The last term on the right side of equation (2) desribes the (known) deviation from equilibrium in the time domain at some particular time $t = 0$.

One seeks a general solution of equation (2) in the form

$$\tilde{\boldsymbol{\phi}}(z, s) = \mathbf{S}(s)\tilde{\boldsymbol{\eta}}(z, s). \tag{4}$$

The objective is to choose **S** so that equation (2) becomes decoupled; that is, independent equations will exist for each of the new dependent variables $\tilde{\eta}_i$. The role of the variables $\tilde{\eta}_i$ is analogous to that of *Riemann invariants* in the method of characteristics.

2.1. DETERMINATION OF S

The first step in the solution process is the choice of the matrix **S**. Using equation (4) to eliminate $\tilde{\boldsymbol{\phi}}$ from equation (2), one obtains

$$s\mathbf{A}^*(s)\mathbf{S}(s)\tilde{\boldsymbol{\eta}}(z, s) + \mathbf{B}\mathbf{S}(s)(\partial/\partial z)\tilde{\boldsymbol{\eta}}(z, s) = \tilde{\mathbf{r}}(z, s) + \mathbf{A}\boldsymbol{\phi}(z, 0). \tag{5}$$

Multiplication throughout by $(\mathbf{A}^*\mathbf{S})^{-1}$—which is equal to $\mathbf{S}^{-1}\mathbf{A}^{*-1}$—yields

$$s\tilde{\boldsymbol{\eta}}(z, s) + \boldsymbol{\Lambda}(s)(\partial/\partial z)\tilde{\boldsymbol{\eta}}(z, s) = s\tilde{\boldsymbol{\eta}}_r(z, s), \tag{6}$$

in which $\boldsymbol{\Lambda}$, important in the following development, is defined by

$$\boldsymbol{\Lambda}(s) = \mathbf{S}^{-1}(s)\mathbf{A}^{*-1}(s)\mathbf{B}\mathbf{S}(s), \tag{7}$$

and $\tilde{\boldsymbol{\eta}}_\mathbf{r}$, introduced for convenience, is defined by

$$\tilde{\boldsymbol{\eta}}_\mathbf{r}(z, s) = (1/s)\mathbf{S}^{-1}(s)\mathbf{A}^{*-1}(s)\{\tilde{\mathbf{r}}(z, s) + \mathbf{A}\boldsymbol{\phi}(z, 0)\}. \tag{8}$$

One now seeks to choose **S** so that $\boldsymbol{\Lambda}$ becomes a simple diagonal matrix, thereby decoupling equation (6) into a set of independent equations, one for each of the dependent variables $\tilde{\eta}_i$. By inspection of the right side of equation (7), it will be possible to make such a choice if the product $\mathbf{A}^{*-1}\,\mathbf{B}$ has real and distinct eigenvalues or if some eigenvalues occur in complex conjugate pairs [28; p. 309]. This will usually be the case with wave-like problems such as those considered herein. The diagonal elements of $\boldsymbol{\Lambda}$ will be the eigenvalues of $\mathbf{A}^{*-1}\,\mathbf{B}$, namely the solution of the eigenvalue (dispersion, characteristic) equation

$$\det(\mathbf{B} - \lambda(s)\mathbf{A}^*(s)) = 0. \tag{9}$$

After having determined $\boldsymbol{\Lambda}$, the matrix **S** consists of the eigenvectors ξ_i belonging to each λ_i. That is

$$\mathbf{S}(s) = (\boldsymbol{\xi}_1(s)\boldsymbol{\xi}_2(s)\cdots\boldsymbol{\xi}_N(s)). \tag{10}$$

For non-dispersive systems—i.e., $\mathbf{C} = \mathbf{O}$—the matrices $\boldsymbol{\Lambda}$ and **S** are exactly the same as those found in the time-domain MOC analysis in Appendix A. For

future reference, note that the matrix $\mathbf{S}$ is not unique: many valid transformations exist.

2.2. DETERMINATION OF $\tilde{\boldsymbol{\eta}}$

The next step in the solution process is the determination of $\tilde{\boldsymbol{\eta}}$. Since $\boldsymbol{\Lambda}$ is diagonal, equation (6) is a set of independent equations, each of the form

$$s\tilde{\eta}_i(z, s) + \lambda_i(s)\partial\tilde{\eta}_i(z, s)/\partial z = s\tilde{\eta}_{ri}(z, s), \quad i = 1, 2, \ldots, N, \tag{11}$$

where λ_i denotes the ith diagonal element of the matrix $\boldsymbol{\Lambda}$.

Consider the homogeneous form of this equation (i.e., $\tilde{\eta}_{ri} \equiv 0$). By inspection, the solution *must* be exponential because no other function is proportional to its own derivative. The general solution of the complete equation may therefore be written as

$$\tilde{\eta}_i(z, s) = \tilde{\eta}_{0i}(s)\, \mathrm{e}^{-sz/\lambda_i(s)} + \tilde{\eta}^*_{ri}(z, s), \quad i = 1, 2, \ldots, N, \tag{12}$$

in which $\tilde{\eta}_{0i}$ is determined from the boundary conditions (see section 2.4) and $\tilde{\eta}^*_{ri}$ denotes the particular solution

$$\tilde{\eta}^*_{ri}(z, s) = \frac{s\, \mathrm{e}^{-sz/\lambda_i(s)}}{\lambda_i(s)} \int^z \tilde{\eta}_{ri}(z^*, s)\, \mathrm{e}^{sz^*/\lambda_i(s)}\, \mathrm{d}z^*, \quad i = 1, 2, \ldots, N. \tag{13}$$

Note that if $\tilde{\eta}_{ri}$ is independent of z: $\tilde{\eta}^*_{ri}(z, s)$ simply equals $\tilde{\eta}_{ri}(s)$.

The vector $\tilde{\boldsymbol{\eta}}$ may now be written as

$$\tilde{\boldsymbol{\eta}}(z, s) = \mathbf{E}(z, s)\tilde{\boldsymbol{\eta}}_{\mathbf{0}}(s) + \tilde{\boldsymbol{\eta}}^*_{\mathbf{r}}(z, s), \tag{14}$$

in which $\mathbf{E}$ is a diagonal matrix, namely

$$\mathbf{E}(z, s) = \begin{pmatrix} \mathrm{e}^{-sz/\lambda_1(s)} & 0 & 0 & \cdot \\ 0 & \mathrm{e}^{-sz/\lambda_2(s)} & 0 & \cdot \\ 0 & 0 & \mathrm{e}^{-sz/\lambda_3(s)} & \cdot \\ \cdot & \cdot & \cdot & \text{etc.} \end{pmatrix}. \tag{15}$$

2.3. GENERAL SOLUTION

To summarize, the general solution of equation (2) can be expressed as

$$\tilde{\boldsymbol{\phi}}(z, s) = \mathbf{S}(s)\mathbf{E}(z, s)\tilde{\boldsymbol{\eta}}_{\mathbf{0}}(s) + \mathbf{S}(s)\tilde{\boldsymbol{\eta}}^*_{\mathbf{r}}(z, s), \tag{16}$$

in which $\mathbf{S}$, $\mathbf{E}$ and $\tilde{\boldsymbol{\eta}}^*_{\mathbf{r}}$ are determined as described in sections 2.1 and 2.2, and $\tilde{\boldsymbol{\eta}}_{\mathbf{0}}$ is determined from boundary conditions in section 2.4.

2.4. BOUNDARY CONDITIONS

Suppose that the Laplace transformed boundary conditions are linear (in $\tilde{\phi}_i$) and are known at the locations $z = 0$ and $z = L$ of the domain $0 \leqslant z \leqslant L$. Then, upon assuming a total of N equations in N unknowns, there will generally be $N/2$ relationships at each end, namely

$$d_{j1}(s)\tilde{\phi}_1(0, s) + d_{j2}(s)\tilde{\phi}_2(0, s) + \cdots + d_{jN}(s)\tilde{\phi}_N(0, s) = \tilde{q}_j(s), \quad j = 1, 2, \ldots, N/2,$$

$$d_{j1}(s)\tilde{\phi}_1(L, s) + d_{j2}(s)\tilde{\phi}_2(L, s) + \cdots + d_{jN}(s)\tilde{\phi}_N(L, s) = \tilde{q}_j(s),$$

$$j = N/2 + 1, N/2 + 2, \ldots, N, \quad (17)$$

in which $\tilde{q}_j$ defines the Laplace transformed boundary excitation and the various d_{ji} are simple coefficients (or functions of s). These may be collected in the matrix $\mathbf{D}$,

$$\mathbf{D}(s) = (\mathbf{d}_1(s) \quad \mathbf{d}_2(s) \quad \cdots \quad \mathbf{d}_N(s))^{\mathrm{T}}, \quad (18)$$

with

$$\mathbf{d}_j(s) = (\mathrm{d}_{j1}(s) \quad \mathrm{d}_{j2}(s) \quad \cdots \quad \mathrm{d}_{jN}(s))^{\mathrm{T}}. \quad (19)$$

The substitution of the general solution (16) into the boundary conditions (17) yields a linear system of N simultaneous equations for the N constants of integration $\tilde{\eta}_{0i}$. The solution of this system is

$$\tilde{\boldsymbol{\eta}}_{\mathbf{0}}(s) = \mathbf{D}^{*-1}(s)\tilde{\mathbf{q}}^*(s), \quad (20)$$

in which the matrix $\mathbf{D}^*$ is defined by

$$\mathbf{D}^*(s) = (\mathbf{d}_1^*(s) \quad \mathbf{d}_2^*(s) \quad \cdots \quad \mathbf{d}_N^*(s))^{\mathrm{T}}, \quad (21)$$

with

$$\mathbf{d}_j^*(s) = \mathbf{E}(0, s)\mathbf{S}^{\mathrm{T}}(s)\mathbf{d}_j(s), \quad j = 1, 2, \ldots, N/2,$$

$$\mathbf{d}_j^*(s) = \mathbf{E}(L, s)\mathbf{S}^{\mathrm{T}}(s)\mathbf{d}_j(s), \quad j = N/2 + 1, N/2 + 2, \ldots, N, \quad (22)$$

and the vector $\tilde{\mathbf{q}}^*$ is defined by

$$\tilde{\mathbf{q}}^*(s) = (\tilde{q}_1^*(s) \quad \tilde{q}_2^*(s) \quad \cdots \quad \tilde{q}_N^*(s))^{\mathrm{T}}, \quad (23)$$

with

$$\tilde{q}_j^*(s) = \tilde{q}_j(s) - \mathbf{d}_j^{\mathrm{T}}(s)\mathbf{S}(s)\tilde{\boldsymbol{\eta}}_{\mathbf{r}}^*(0, s), \quad j = 1, 2, \ldots, N/2,$$

$$\tilde{q}_j^*(s) = \tilde{q}_j(s) - \mathbf{d}_j^{\mathrm{T}}(s)\mathbf{S}(s)\tilde{\boldsymbol{\eta}}_{\mathbf{r}}^*(L, s), \quad j = N/2 + 1, N/2 + 2, \ldots, N. \quad (24)$$

2.5. COMPLETE SOLUTION

After having deduced $\tilde{\boldsymbol{\eta}}_{\mathbf{0}}$ from the linear boundary conditions, the complete solution may be expressed as (substitution of equation (20) into equation (16)),

$$\tilde{\boldsymbol{\phi}}(z, s) = \mathbf{S}(s)\mathbf{E}(z, s)\mathbf{D}^{*-1}(s)\tilde{\mathbf{q}}^*(s) + \mathbf{S}(s)\tilde{\boldsymbol{\eta}}_{\mathbf{r}}^*(z, s), \quad (25)$$

in which $\mathbf{S}$, $\mathbf{E}$, $\mathbf{D}^*$, $\tilde{\mathbf{q}}^*$ and $\tilde{\boldsymbol{\eta}}_{\mathbf{r}}^*$ are defined by equations (10), (15), (21–22), (23–24) and (13) respectively.

Equation (25) is valid for any values of s ($s \neq 0$) and z ($0 \leqslant z \leqslant L$). When it is evaluated with constant z and varying s, the frequency spectrum of the quantity ϕ_i is found at the location z. Alternatively, by evaluating it with constant s and varying z, one obtains the "mode shape" of quantity ϕ_i at the frequency s.

Green functions can be derived by taking spatial Dirac delta functions for $\mathbf{r}(z, t)$; see e.g., reference [29]. In many practical applications, however, there is no spatially distributed excitation $\mathbf{r}(z, t)$ and, moreover, it is acceptable to neglect any initial disturbance $\boldsymbol{\phi}(z, 0)$—except when deliberately introduced as in snap-back tests, for example. In such cases, $\tilde{\boldsymbol{\eta}}_{\mathbf{r}}$ defined in (8) is $\mathbf{0}$—so that $\tilde{\boldsymbol{\eta}}_{\mathbf{r}}^{*} = \mathbf{0}$ and $\tilde{\mathbf{q}}^{*} = \tilde{\mathbf{q}}$—and equation (25) simplifies to

$$\tilde{\boldsymbol{\phi}}(z, s) = \mathbf{S}(s)\mathbf{E}(z, s)\mathbf{D}^{*-1}(s)\tilde{\mathbf{q}}(s). \tag{26}$$

This equation is used in the examples presented in sections 3 and 4. The system is excited only at the boundaries through the vector $\tilde{\mathbf{q}}$. The boundary conditions can be changed through the matrix $\mathbf{D}$ and consequently $\mathbf{D}^{*}$. The matrices $\mathbf{E}$ and $\mathbf{S}$ define the acoustic properties of the system (see section 2.6).

2.6. TRANSFER MATRIX

The vibrational characteristics of the system, without any influences of boundary conditions, are best described by the *transfer matrix* $\mathbf{M}$,

$$\mathbf{M}(z, s) = \mathbf{S}(s)\mathbf{E}(z, s)\mathbf{S}^{-1}(s), \tag{27}$$

which is obtained from equation (26) by expressing $\tilde{\boldsymbol{\phi}}(z, s)$ in terms of $\tilde{\boldsymbol{\phi}}(0, s)$ through

$$\tilde{\boldsymbol{\phi}}(z, s) = \mathbf{M}(z, s)\tilde{\boldsymbol{\phi}}(0, s), \tag{28}$$

upon noting that $\mathbf{E}(0, s) = \mathbf{I}$.

An alternative method of calculation, not used herein, is to solve the boundary conditions (17) and the transfer equation (27), with $z = L$, simultaneously for $\tilde{\boldsymbol{\phi}}(0, s)$ and $\tilde{\boldsymbol{\phi}}(L, s)$.

3. APPLICATION A: FLEXURAL VIBRATION OF A FLUID-FILLED PIPE

The use of the analysis is illustrated first for the case of a fluid-filled pipe, closed at both ends and subjected to *lateral* excitation. The pipe is straight and has linearly elastic walls. The excitation sources are at the ends and act perpendicularly to the pipe axis. By restricting consideration to small deflections, one can neglect axial movement of the fluid and the pipe [30]. Thus the only effect of the contained fluid is to increase the mass in comparison with that for an empty pipe. With this adjustment, the physical conditions are identical to those for Timoshenko beams.

The equations of motion can be found elsewhere (see, e.g., references [31, 32]). In the notation of equation (1), they may be written as

$$\mathbf{A} = \begin{pmatrix} 1 & 0 & 0 & 0 \\ 0 & 1/\kappa^2 GA_s & 0 & 0 \\ 0 & 0 & 1 & 0 \\ 0 & 0 & 0 & 1/EI_s \end{pmatrix}, \quad \mathbf{B} = \begin{pmatrix} 0 & c_S^2/\kappa^2 GA_s & 0 & 0 \\ 1 & 0 & 0 & 0 \\ 0 & 0 & 0 & c_B^2/EI_s \\ 0 & 0 & 1 & 0 \end{pmatrix},$$

$$\mathbf{C} = \begin{pmatrix} 0 & 0 & 0 & 0 \\ 0 & 0 & 1 & 0 \\ 0 & -c_B^2/EI_s & 0 & 0 \\ 0 & 0 & 0 & 0 \end{pmatrix}, \quad \boldsymbol{\phi} = \begin{pmatrix} V \\ Q \\ \psi \\ M \end{pmatrix} \quad \text{and} \quad \mathbf{r} = \mathbf{0}, \tag{29}$$

in which the dependent variables are the lateral velocity V, the lateral shear force Q, the angular velocity ψ and the bending moment M. The properties of the fluid and the pipe are defined in the Nomenclature (Appendix D) and the uncoupled ($|s| = \infty$) shear and bending wave speeds satisfy

$$c_S^2 = \kappa^2 GA_s/(\rho_s A_s + \rho_f A_f) \quad \text{and} \quad c_B^2 = E/\rho_s. \tag{30}$$

Following the sequence outlined in section 2, one can first solve equation (9), which, in this instance, is the dispersion relation for lateral wave propagation:

$$(1 + \kappa^2 GA_s/\rho_s I_s s^2)\lambda^4(s) - (c_S^2 + c_B^2)\lambda^2(s) + c_S^2 c_B^2 = 0. \tag{31}$$

The solution of this equation, expressed in real frequencies f by taking $s = 2\pi f\mathrm{i}$, is

$$\lambda_{1,2}^2(f) = \frac{(c_S^2 + c_B^2) - \{(c_S^2 - c_B^2)^2 + 4(f_c/f)^2 c_S^2 c_B^2\}^{1/2}}{2\{1 - (f_c/f)^2\}},$$

$$\lambda_{3,4}^2(f) = \frac{(c_S^2 + c_B^2) + \{(c_S^2 - c_B^2)^2 + 4(f_c/f)^2 c_S^2 c_B^2\}^{1/2}}{2\{1 - (f_c/f)^2\}}, \tag{32}$$

where

$$f_c^2 = \kappa^2 GA_s/4\pi^2 \rho_s I_s. \tag{33}$$

Note that f_c is independent of the contained fluid. The special case $f = f_c$ gives

$$\lambda_{1,2}^2(f_c) = (1/c_S^2 + 1/c_B^2)^{-1}. \tag{34}$$

The eigenvalues $\lambda_{1,2}$ are the frequency dependent (dispersive) wave speeds (phase velocities) in a Timoshenko beam. The eigenvalues $\lambda_{3,4}$ are imaginary numbers when $f < f_c$; they represent a second mode of vibration that exists only at frequencies higher than the cut-on frequency f_c. Such high frequencies are not considered herein. It is noted that at very high frequencies ($f \to \infty$), $\lambda_{1,2}$ tend to $\pm c_S$ and $\lambda_{3,4}$ tend to $\pm c_B$, which are the speeds of propagation of discontinuities in Q (and V) and in M (and ψ) respectively [31–33].

The matrix $\mathbf{S}$, consisting of the eigenvectors $\boldsymbol{\xi}_i$ belonging to λ_i, is obtained by solving equation (7). This matrix is given in Appendix B.

An important feature of the frequency domain analysis is that the matrix **S** is a full(y-coupling) matrix. This contrasts with the approach taken in MOC analyses, where $\mathbf{C}\boldsymbol{\phi}$ (in equation (1)) has to be treated (numerically) as a "right side" term in the governing equations. That is, it contributes to the compatibility relationships, but not to the paths along which these relationships are regarded as applicable.

Hysteretic damping is introduced in the analysis through a complex-valued modulus of elasticity [34, see pp. 195–204].

3.1. FLUID AND SOLID PROPERTIES

In the following particular examples, the fluid and solid properties are as listed in Table 1. They are those of a laboratory apparatus described by Vardy and Fan [35]. In that apparatus, a 4·5 m long pipe of 60 mm outer diameter is closed at both ends and hangs horizontally on two long, steel wires. In some experiments, it is filled with water; in others, it contains only air. The pipe can be struck axially or laterally by a 5 m long steel rod moving horizontally in the direction of its own axis—see Figures 1(a), and 3(a) of section 4.1.

Damping, introduced in the calculations by taking a loss factor $\eta = 0{\cdot}01$ in the complex modulus $E = 168\ (1 + \eta\mathrm{i})$ GPa, reduces the amplitudes of vibration near resonance.

3.2. EXAMPLE A1: DISCRETE IMPACT

In example A1, which is a numerical simulation of the physical experiment, the pipe is supported freely in a horizontal plane. An assumed constant lateral force $Q(0, t) = F_{\mathrm{rod}}$ exists at one end for a finite duration $0 < t < T$, causing

TABLE 1

Geometrical and material properties of Dundee single pipe apparatus [35]

Steel pipe	End caps
$L = 4502$ mm	$L_0 = 60$ mm
$R = 26{\cdot}01$ mm	$m_0 = 1{\cdot}312$ kg
$e = 3{\cdot}945$ mm	$L_L = 5$ mm
$E = 168$ GPa	$m_L = 0{\cdot}3258$ kg
$\rho_s = 7985$ kg/m^3	
$\nu = 0{\cdot}29$	Air
$\kappa^2 = 0{\cdot}53$	
$A_f = 2125$ mm^2	$K_a = P \ll E$
$A_s = 694$ mm^2	$\rho_a = 1{\cdot}2$ kg/m^3
$I_s = 272900$ mm^4	
$\eta = 0{\cdot}01$	Water
$\xi = 0{\cdot}002$	
	$K = 2{\cdot}14$ GPa
	$\rho_f = 999$ kg/m^3
	$\mu = 0{\cdot}001$ Pas

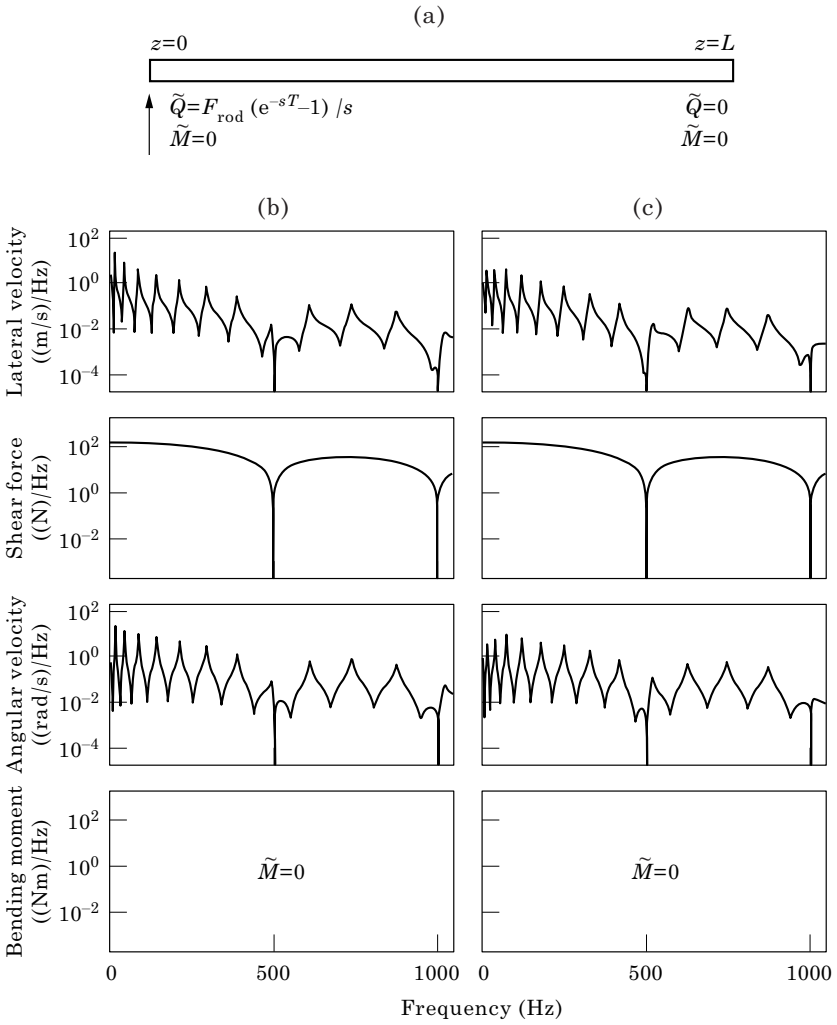

Figure 1. Discrete lateral impact of free hanging pipe: (a) boundary conditions in frequency domain; (b) frequency response of air-filled pipe; (c) frequency response of water-filled pipe.

flexural waves to propagate along the pipe. The remaining boundary conditions at the ends $z = 0$ and $z = L$ are $Q(L, t) = 0$, $M(0, t) = 0$ and $M(L, t) = 0$. The Laplace transformed applied load is then

$$\tilde{Q}(0, s) = (F_{\text{rod}}/s)(e^{-sT} - 1). \tag{35}$$

The magnitude and duration of the applied pulse are $F_{\text{rod}} \approx 80$ kN and $T \approx 2$ ms. With these boundary conditions, the matrix of boundary coefficients $\mathbf{D}$ and the excitation vector $\tilde{\mathbf{q}}$ are

$$\mathbf{D} = \begin{pmatrix} 0 & 1 & 0 & 0 \\ 0 & 0 & 0 & 1 \\ 0 & 1 & 0 & 0 \\ 0 & 0 & 0 & 1 \end{pmatrix} \quad \text{and} \quad \tilde{\mathbf{q}}(s) = \begin{pmatrix} \tilde{Q}(0, s) \\ 0 \\ 0 \\ 0 \end{pmatrix}. \tag{36}$$

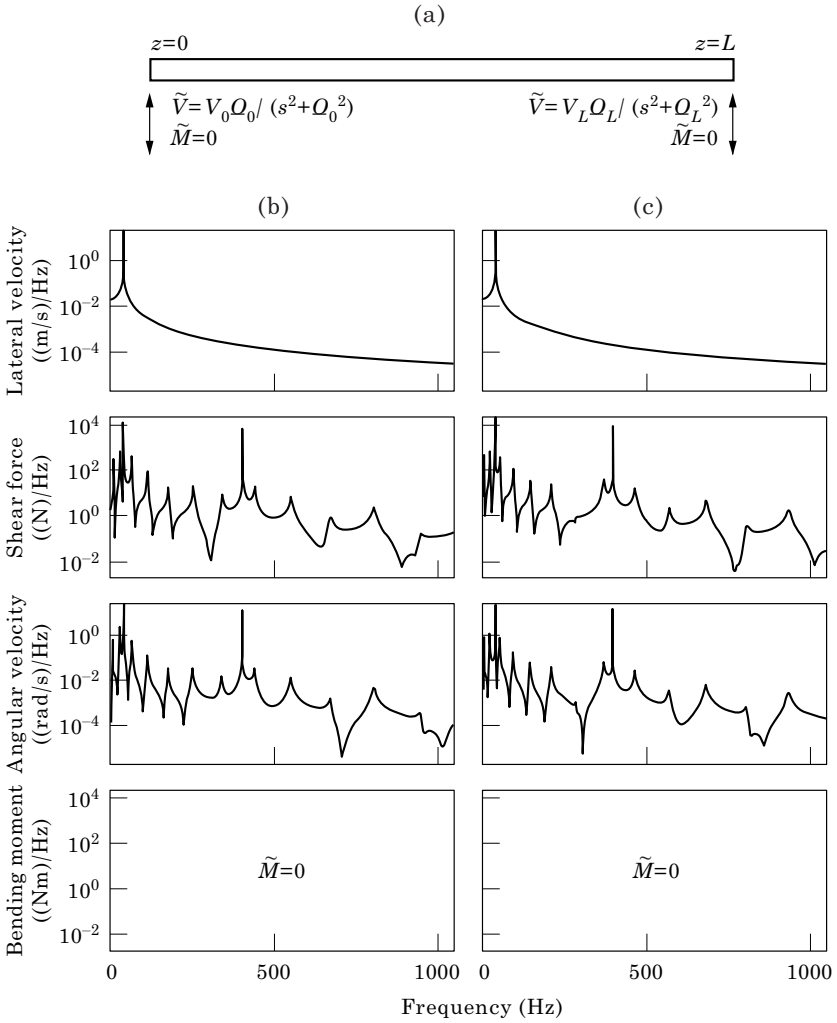

Figure 2. Biharmonic lateral vibration of hinged supports: (a) boundary conditions in frequency domain; (b) frequency response of air-filled pipe; (c) frequency response of water-filled pipe.

The first two rows of **D** apply at $z = 0$ and the last two apply at $z = L$. This convention is used in all four examples herein.

3.2.1. *Solution*

Predicted frequency spectra, i.e., $\mathrm{mod}(\tilde{\phi}_i(0, s))$ for $i = 1, 2, 3$ and 4, are shown in Figures 1(b) and 1(c) for air-filled and water-filled pipes respectively. The frequency is $f = s/(2\pi\mathrm{i})$ and the frequency resolution Δf is 1 Hz in Figures 1–3. The cut-on frequency f_c is 17 kHz.

The bending moment and shear force curves are included for completeness; these are prescribed quantities at $z = 0$. The two downward peaks in the shear

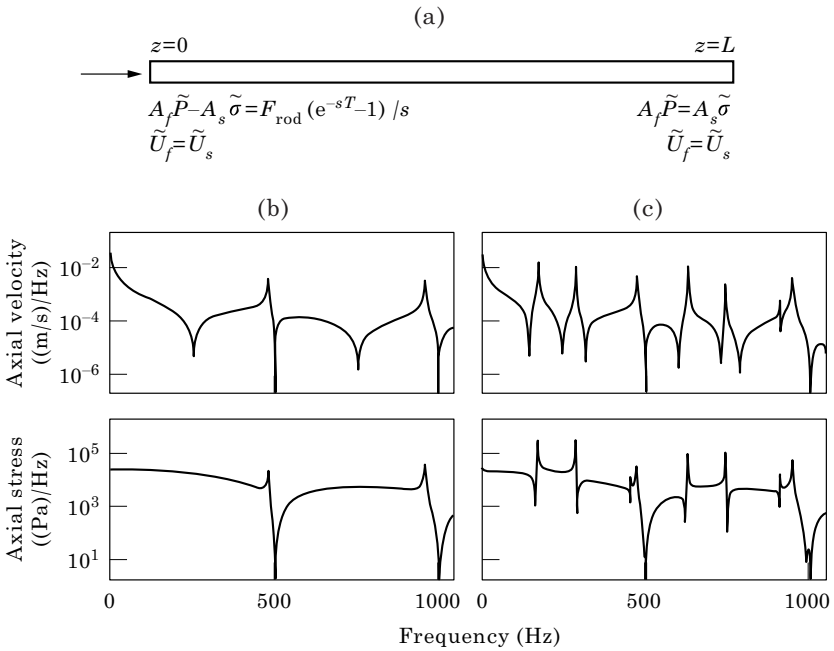

Figure 3. Discrete axial impact of free hanging pipe: (a) boundary conditions in frequency domain; (b) frequency response of air-filled pipe; (c) frequency response of water-filled pipe.

force correspond to the basic frequency $1/T = 500$ Hz representing the finite duration of the square pulse excitation.

The upward peaks in the velocities represent the natural frequencies of the system. Because there is no excitation around 500 and 1000 Hz frequencies, any natural frequencies close to these values cannot be detected.

The natural frequencies of the water-filled pipe are about 15% lower than those of the air-filled pipe. This is due to the extra mass of the water, the square root of the ratio of the two masses being $\{(\rho_s A_s + \rho_a A_f)/(\rho_s A_s + \rho_f A_f)\}^{1/2} = 0{\cdot}85$.

The calculated natural frequencies in Table 2 are equal to those derived from Huang's [26, equation (36)] analytical solutions for a freely vibrating Timoshenko beam.

The measured natural frequencies in Table 2 are obtained from discrete Fourier transformations applied to axial-strain histories of 1·5 s duration and consisting of 15 000 samples. The measured values are close to those derived theoretically.

The impact end of the Dundee test pipe is sealed with a solid plug of length $L_0 = 60$ mm. The results in Table 2 indicate that long (low frequency) waves reflect from the free end of the plug, whereas short (high frequency) waves reflect from the plug itself (that is the plug–pipe junction).

It is noted that the nth natural frequency f_n of a free Timoshenko beam is associated with the wavelength $4L/(2n + 1)$. A good approximation of f_n can be

TABLE 2

Natural frequencies (*in* Hz) *of lateral vibration of pipe with free ends*

Air-filled pipe			Water-filled pipe		
Measurement	Calculation with length L	Calculation with length $L + L_0$	Measurement	Calculation with length L	Calculation with length $L + L_0$
15	16	16	13	14	13
41	44	43	36	37	36
81	86	84	70	73	71
135	141	138	116	120	117
202	210	205	173	179	174
281	291	284	241	248	242
373	385	375	320	328	320
478	491	478	411	418	408
595	607	592	510	518	505
723	735	717	619	627	611
859	872	851	737	744	726
1008	1019	995	864	870	849
1170	1175	1147	999	1003	979

found by replacing the wave speeds $\lambda_{1,2}$ in equation (32) by the product of wavelength and frequency—$(4L/(2n + 1))f$—and then solving for f.

3.3. EXAMPLE A2: HARMONIC EXCITATION

The physical configuration used for example A2, which is a numerical test case, is the same as for example A1, but the boundary conditions are different. The ends of the pipe are hinged to supports that are vibrating harmonically, but with different frequencies. That is, $\tilde{M}(0, s) = 0$, $\tilde{M}(L, s) = 0$, $\tilde{V}(0, s) = V_0\mathcal{L}\{\sin(\Omega_0 t)\} = V_0\Omega_0/(s^2 + \Omega_0^2)$ and $\tilde{V}(L, s) = V_L\mathcal{L}\{\sin(\Omega_L t)\} = V_L\Omega_L/(s^2 + \Omega_L^2)$ where $V_0 = 5{\cdot}0$ m/s, $V_L = 0{\cdot}5$ m/s, $\Omega_0 = 2\pi * 40$ Hz and $\Omega_L = 2\pi * 400$ Hz or, in matrix notation,

$$\mathbf{D} = \begin{pmatrix} 1 & 0 & 0 & 0 \\ 0 & 0 & 0 & 1 \\ 1 & 0 & 0 & 0 \\ 0 & 0 & 0 & 1 \end{pmatrix} \quad \text{and} \quad \tilde{\mathbf{q}}(s) = \begin{pmatrix} V_0\Omega_0/(s^2 + \Omega_0^2) \\ 0 \\ V_L\Omega_L/(s^2 + \Omega_L^2) \\ 0 \end{pmatrix}. \tag{37}$$

TABLE 3
Natural frequencies (in Hz*) of lateral vibration of pipe with hinged ends*

Air-filled pipe (calculated)	Water-filled pipe (calculated)
7	6
28	24
63	54
112	95
174	148
249	212
336	287
436	371
547	466
669	570
801	683
943	804

This example has been chosen to demonstrate the method's ability to handle arbitrary linear boundary excitations. In purely harmonic analyses, the boundary excitation is assumed to have a constant amplitude, independent of f. The excitation is then white noise, which corresponds to a Dirac pulse in the time domain. In the present method, instead of the Dirac pulse or the white noise, an actual (i.e., measured) excitation of the system is used. This means that the amplitude of the excitation is frequency dependent. Also, the calculated frequency spectra include the transient response to impact at $t = 0$ (start-up phenomena), so that, in principle, early time histories can be obtained from (numerical) inverse Fourier and Laplace transformations.

3.3.1. *Solution*

Predicted frequency spectra ($z = 0$) are shown in Figures 2(b) and 2(c) for air-filled and water-filled pipes respectively. The imposed 40 and 400 Hz peaks are clearly visible as well as the natural frequencies of the system itself.

The natural frequencies in Table 3 are the same as those obtained from Huang's [26, equation (35)] analytical expression for a hinged Timoshenko beam. Again, the natural frequencies are about 15% lower in the water-filled pipe than in the air-filled pipe.

It is noted that the nth natural frequency f_n of a hinged Timoshenko beam is associated with the wavelength $2L/n$. Values of f_n can be found by replacing the wave speeds $\lambda_{1,2}$ in equation (32) by the product of wavelength and frequency—$(2L/n)f$—and then solving for f.

4. APPLICATION B: AXIAL VIBRATION OF A FLUID-FILLED PIPE

The use of the analysis is now illustrated for the case of a fluid-filled pipe subjected to *axial* excitation. Once again, the pipe is straight and has linearly elastic walls. In one example, it is closed at both ends; in the other, waterhammer and pipe vibration in a reservoir–pipe–valve system is considered. The excitation sources are at the ends and act axially. No lateral deflections exist, but strong interactions occur between the liquid and the pipe. The principal interactions occur at the ends, but there is also *Poisson coupling* and *friction coupling* along the pipe.

The equations of motion have been given elsewhere [36–40]. In the notation of equation (1), they may be written as

$$\mathbf{A} = \begin{pmatrix} 1 & 0 & 0 & 0 \\ 0 & 1/\rho_f c_f^2 & 0 & 0 \\ 0 & 0 & 1 & 0 \\ 0 & (\nu/E)(R/e) & 0 & -1/\rho_s c_s^2 \end{pmatrix}, \quad \mathbf{B} = \begin{pmatrix} 0 & 1/\rho_f & 0 & 0 \\ 1 & 0 & -2\nu & 0 \\ 0 & 0 & 0 & -1/\rho_s \\ 0 & 0 & 1 & 0 \end{pmatrix},$$

$$\mathbf{C} = \begin{pmatrix} f_f & 0 & -f_f & 0 \\ 0 & 0 & 0 & 0 \\ -f_s & 0 & f_s + D_s & 0 \\ 0 & 0 & 0 & 0 \end{pmatrix}, \quad \boldsymbol{\phi} = \begin{pmatrix} U_f \\ P \\ U_s \\ \sigma \end{pmatrix} \quad \text{and} \quad \mathbf{r} = \mathbf{0}, \tag{38}$$

in which the dependent variables are the axial velocities U_f and U_s, the fluid pressure P and the axial stress σ in the fluid (f) and solid (s) respectively. The properties of the fluid and the pipe are defined in the Nomenclature (Appendix D) and the *uncoupled* axial wave speeds in the two media satisfy

$$c_f^2 = (K/\rho_f)/\{1 + (1 - \nu^2)2KR/Ee\} \quad \text{and} \quad c_s^2 = E/\rho_s. \tag{39}$$

Matrix **C** contains the coefficients for linear friction coupling and for viscous structural damping. It is noted that $f_s = \{(R\rho_f)/(2e\rho_s)\}f_f$ for thin-walled circular pipes.

Following the same sequence as before, one can first solve equation (9), which in this case is the dispersion equation for axial wave propagation:

$$a(s)\lambda^4(s) + b(s)\lambda^2(s) + c = 0. \tag{40}$$

Here

$$a(s) = 1 + (f_f + f_s + D_s)(1/s) + f_f D_s/s^2, \tag{40a}$$

$$b(s) = -\gamma^2 - \left\{ \left(c_s^2 - \nu(1-2\nu)\frac{R}{e}\frac{\rho_f}{\rho_s}c_f^2 \right) f_f + (1-2\nu)c_f^2 f_s + c_f^2 D_s \right\} \frac{1}{s}, \qquad (40b)$$

$$c = c_f^2 c_s^2 \qquad (40c)$$

and

$$\gamma^2 = (1 + 2\nu^2(\rho_f/\rho_s)(R/e))c_f^2 + c_s^2. \qquad (41)$$

The system is non-dispersive when $\mathbf{C} = \mathbf{O}$, because the wave speeds λ_i are then independent of s:

$$\lambda_{1,2}^2 = \tfrac{1}{2}\{\gamma^2 - (\gamma^4 - 4c_f^2 c_s^2)^{1/2}\}, \quad \lambda_{3,4}^2 = \tfrac{1}{2}\{\gamma^2 + (\gamma^4 - 4c_f^2 c_s^2)^{1/2}\}. \qquad (42)$$

The pressure wave speed $\lambda_{1,2}$ in equation (42) is smaller than the classical value c_f, because the latter does not allow for the axial inertia of the pipe wall. The axial stress wave speed $\lambda_{3,4}$ in equation (42) is larger than the classical value c_s, because the latter does not account for pressure changes provoked by axial stresses.

The matrix $\mathbf{S}$ obtained from equation (7) is given in Appendix C.

4.1. EXAMPLE B1: DISCRETE IMPACT

In example B1, which is a numerical simulation of the physical experiment of Vardy and Fan [35], the pipe of example A is freely supported in a horizontal plane (see Figure 3(a)). A constant force $F_{\text{rod}} \approx 9{\cdot}4$ kN is suddenly applied axially at one end ($z = 0$) and persists for a duration $T = 2L/c_s \approx 2$ ms, causing axial waves to propagate along the pipe. At the other end of the pipe, there is no restraint except for inertia of the end cap, and so the stipulated force is zero. Both ends of the pipe are closed so $\tilde{U}_f(0, s) = \tilde{U}_s(0, s)$ and $\tilde{U}_f(L, s) = \tilde{U}_s(L, s)$. With these boundary conditions, the matrix $\mathbf{D}$ and vector $\tilde{\mathbf{q}}$ are

$$\mathbf{D} = \begin{pmatrix} 1 & 0 & -1 & 0 \\ 0 & A_f & sm_0 & -A_s \\ 1 & 0 & -1 & 0 \\ 0 & A_f & -sm_L & -A_s \end{pmatrix} \quad \text{and} \quad \tilde{\mathbf{q}}(s) = \begin{pmatrix} 0 \\ (F_{\text{rod}}/s)(\mathrm{e}^{-sT} - 1) \\ 0 \\ 0 \end{pmatrix}. \qquad (43)$$

Damping is introduced in the calculations by taking $f_f = 0{\cdot}12$ Hz, $f_s = 0{\cdot}05$ Hz and $D_s = 18$ Hz in matrix $\mathbf{C}$. The fluid friction coefficient f_f is taken ten times larger than $8\mu/(\rho_f R^2)$, which is its value in steady laminar flow, to allow for unsteady turbulent friction losses [43]. The structural damping coefficient D_s equals $2\xi c_s$ (per m) after Budny *et al.* [38]. However, the value of the damping ratio ξ is taken ten times smaller than in reference [38], because damping is much smaller in the freely suspended pipe considered herein than in Budny's pipe system. The influence of damping is visible in the results near (anti)resonance and at frequencies below 5 Hz.

4.1.1. *Solution*

Predicted frequency spectra, i.e., $\mathrm{mod}(\tilde{\phi}_i(0, 2\pi \mathrm{i} f))$ for $i = 3$ and 4, are shown in Figures 3(b) and 3(c) for air-filled and water-filled pipes respectively. The curves of the air-filled pipe show resonance frequencies at 478 and 957 Hz. Due to the masses m_0 and m_L of the end caps, these values differ from the theoretical values $c_s/(2L) = 509$ Hz and $c_s/L = 1019$ Hz. The curves of the water-filled pipe show many more resonance frequencies (approximately $c_f/(2L) = 151$ Hz + higher harmonics), because the pulsating water column interacts strongly with the vibrating pipe. Note that the velocity spectra at the pipe ends are the same for the fluid and the pipe—because of the no-separation condition.

The resonance frequencies observed from Figure 3(c) are listed in Table 4, where, as an experimental validation of the present method, they are compared with data measured in impact tests [27]. The measured frequencies were obtained from a discrete Fourier transformation applied to a 1 s pressure history consisting of 10 000 samples. It is seen that the analysis picks up all the resonance frequencies in the system. The lumped end masses in the calculation

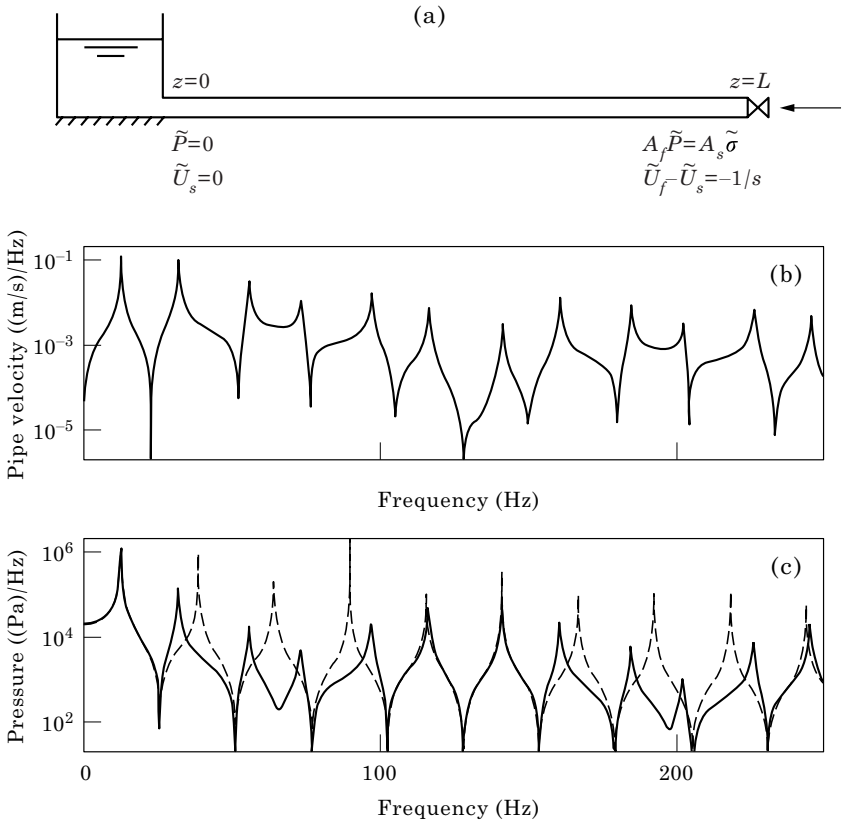

Figure 4. Instantaneous closure of unrestrained valve in reservoir–pipe–valve system: (a) boundary conditions in frequency domain; (b–c) calculated frequency spectra at valve of (b) axial pipe velocity and (c) pressure, (—) with FSI, (- - -) classical waterhammer.

TABLE 4
Natural frequencies (in Hz*) of axial vibration of water-filled pipe with free ends*

Measurement	Calculation without end masses	Difference (%)	Calculation with end masses	Difference (%)
173	172	−0·6	171	−1·2
289	286	−1·0	285	−1·4
459	453	−1·3	453	−1·3
485	493	+1·6	472	−2·7
636	633	−0·5	626	−1·6
750	741	−1·2	740	−1·3
918	907	−1·2	906	−1·3
968	980	+1·2	944	−2·5

have little influence on the fluid modes, but they significantly lower the structural modes (the 485 Hz and 968 Hz modes in the measurements). The agreement between theory and experiment is good (differences less than 3%).

4.2. EXAMPLE B2: WATERHAMMER WITH FSI

In example B2, the pipe is fixed to an immovable, constant pressure reservoir at its upstream end and has a valve at its unrestrained downstream end (see Figure 4(a)). For convenience, the pipe is assumed to have the same properties as those in previous work (numerical benchmark problem of Lavooij and Tijsseling [39, Figure 7]) (see Table 5). It is noted that the cut-on frequency of the pipe's first lobar mode ("ovalizing") is 18 Hz [13, p. 23; 41, p. 418], but that the influence of lobar modes on axial vibration is small at low frequencies [13, p. 24].

At the time $t = 0$, the liquid and pipe wall at the valve ($z = L$) are suddenly excited by an imposed relative velocity $U_f(L, t) - U_s(L, t)$ equal to -1 m/s. This corresponds to an instantaneous closure of an unrestrained valve, thereby providing FSI junction coupling.

After Laplace transformation, the kinematic boundary condition at the valve is

$$\tilde{U}_f(L, s) - \tilde{U}_s(L, s) = -1/s \tag{44}$$

and the equilibrium condition is

$$A_f\tilde{P}(L, s) = A_s\tilde{\sigma}(L, s) + sm_L\tilde{U}_s(L, s), \tag{45}$$

where m_L is the mass of the valve.

TABLE 5

Geometrical and material properties of reservoir–pipe–valve system [39, *Figure* 7]

Steel pipe	Water
$L = 20$ m	$K = 2{\cdot}1$ GPa
$R = 398{\cdot}5$ mm	$\rho_f = 1000$ kg/m^3
$e = 8$ mm	$\mu = 0{\cdot}001$ Pas
$E = 210$ GPa	–
$\rho_s = 7900$ kg/m^3	–
$\nu = 0{\cdot}30$	–
$m_L = 0$ kg	–
$\xi = 0{\cdot}002$	–

At the other end of the pipe, the constant pressure boundary condition is

$$\tilde{P}(0, s) = 0 \tag{46}$$

and the pipe is assumed to remain stationary at its connection with the reservoir: i.e.,

$$\tilde{U}_s(0, s) = 0. \tag{47}$$

Damping is introduced in the calculations by taking $f_f = 0{\cdot}0005$ Hz, $f_s = 0{\cdot}002$ Hz and $D_s = 21$ Hz in matrix $\mathbf{C}$. For reasons given in example B1, the fluid friction coefficient f_f is ten times larger than its value in steady laminar flow and the value of the damping ratio ξ in $D_s = 2\xi c_s$ (per m) is taken ten times smaller than in reference [38]. Damping diminishes the resonance peaks and the anti-resonance dips.

4.2.1. *Solution*

Predicted frequency spectra for the pipe velocity and the pressure at the valve are shown in Figures 4(b) and 4(c) respectively. Figure 4(c) (solid line) is representative for both liquid and pipe, because the pressure at the valve is proportional to the pipe stress at the valve through equation (45), with $m_L = 0$. The broken line in Figure 4(c) is the classical waterhammer solution obtained from uncoupled equations (38) (with $\nu = 0$ and $f_s = 0$) and boundary conditions (44) (with $\tilde{U}_s \equiv 0$) and (46). The frequency resolution Δf in Figure 4 is 0·25 Hz.

For verification, the present results have been compared with results of the MOC–FFT method (see, e.g., references [35, 42]). The latter results have been obtained by the straight-forward application of a discrete Fourier transform to a time history calculated by the MOC. The duration of the time history was 2 s and the numerical time step was $\Delta t = 0{\cdot}5$ ms. The MOC–FFT method yields the same resonant frequencies as the method presented herein.

TABLE 6

Natural frequencies (in Hz*) in reservoir–pipe–valve system with instantaneously closed, unrestrained valve*

FSI calculation	Fluid $c_f(\nu = 0{\cdot}30)/(4L)$ odd harmonics	Fluid $c_f(\nu = 0)/(4L)$ odd harmonics	Pipe $c_s/(4L)$ odd harmonics
12	13	13	–
32	39	38	–
56	66	64	–
73	–	–	64
97	92	90	–
116	118	115	–
141	144	141	(129 even)
161	171	167	–
185	197	192	–
202	–	–	193
226	223	218	–
245	249	244	–

These FSI frequencies are listed in Table 6 together with the natural frequencies given by classical waterhammer and beam theories. Roughly, the waterhammer frequency $c_f/(4L) = (1049 \text{ m/s})/(80 \text{ m}) = 13$ Hz and the beam frequency $c_s/(4L) = (5156 \text{ m/s})/(80 \text{ m}) = 64$ Hz and their odd higher harmonics dominate the spectrum. The pressure wave speed c_f given by equation (39) is used in conventional waterhammer analyses when the pipeline is anchored against axial motion (zero axial strain). When the pipeline has expansion joints throughout its length (zero axial stress) Poisson's ratio is taken as zero in equation (39) so that $c_f = 1026$ m/s. Natural frequencies based on this latter value of c_f are given in the third column of Table 6. The FSI (Poisson-coupled) wave speeds are found from equations (42) as $\lambda_1 = 1025$ m/s and $\lambda_3 = 5281$ m/s.

There is a tendency of the coupled values (left column in Table 6) to deviate from the uncoupled values (right three columns in Table 6), when the natural frequencies of liquid and pipe are close to each other. This is the case for the third and eighth fluid harmonics, which have frequencies very close to those of the first and second pipe harmonics, respectively. Figure 4(c) shows that the

classical pressure spectrum (broken line) changes completely in the vicinity of the structural frequencies 64 Hz and 193 Hz as a result of FSI (solid line).

In a classical waterhammer calculation [18, 19], the valve is assumed to be immovable and any liquid–pipe coupling is ignored. In that case, after valve closure, the liquid column comprises an *open–closed* hydraulic system with a fundamental frequency of $c_f/(4L)$. The pipe is *fixed–fixed* (theoretically), which gives a fundamental frequency of $c_s/(2L)$ (with *even* harmonics).

If the valve is able to move, calculations with FSI (junction coupling) are required. Liquid and pipe variables are coupled at the valve through hybrid boundary conditions in which both displacements (or velocities) and forces (or pressures and stresses) are described.

It is interesting to see that, despite FSI, the liquid column still resembles an *open–closed* system, whereas, due to unrestraining the valve, the pipe becomes nearly *fixed–free* (with *odd* harmonics). Apparently, the valve displacements are relatively small for the vibration of the liquid column, whereas they are relatively large for the vibration of the pipe.

5. CONCLUSIONS

1. An analytical model of the frequency response of liquid-filled pipes has been presented, account being taken of fluid/structure interactions due to linear friction, Poisson and junction coupling.

2. Close analogies have been drawn with the time-domain method of characteristics (MOC). The same eigenvalues, eigenvectors and transformation matrices apply in both methods, in non-dispersive systems.

3. The frequency domain model permits a more accurate representation of frequency-dependent terms and dispersive terms than is possible with MOC.

4. The model is more accurate and, for some purposes, more convenient than the MOC–FFT approach in which results are obtained by MOC in the time domain and transformed into the frequency domain by FFT.

5. The model has been validated by comparison with analytical, experimental and MOC–FFT evidence for lateral and axial vibrations of a fluid-filled straight pipe excited by instantaneous impact and biharmonic support vibration.

6. The model includes transient excitation spectra and so has the potential for numerical transformation into the time domain for arbitrarily varied, linear (in the dependent variables), boundary conditions.

ACKNOWLEDGMENTS

The authors thank the Engineering and Physical Sciences Research Council (UK) [Grant ref: GR/J 54857] and the Yunnan Provincial Science and Technology Commission (PRC) for financial support of this research. Ernie Kuperus and Colin Stark assisted in the experimental part of the work. The reviewers are thanked for their criticisms and valuable suggestions for improving the paper.

REFERENCES

1. A. S. TIJSSELING 1996 *Journal of Fluids and Structures* **10**, 109–146. Fluid–structure interaction in liquid-filled pipe systems: a review.
2. D. C. WIGGERT 1996 *Proceedings of the* 18*th IAHR Symposium on Hydraulic Machinery and Cavitation*, *Valencia, Spain, September*, 58–67, ISBN 0-7923-4210-0. Fluid transients in flexible piping systems (a perspective on recent developments).
3. A. F. D'SOUZA and R. OLDENBURGER 1964 *ASME Journal of Basic Engineering* **86**, 589–598. Dynamic response of fluid lines.
4. D. H. WILKINSON 1978 *Proceedings of the BNES International Conference on Vibration in Nuclear Plant*, *Keswick*, *UK*, *May*, *Paper* **8.5**, 863–878. Acoustic and mechanical vibrations in liquid-filled pipework systems.
5. M. EL-RAHEB 1981 *Journal of Sound and Vibration* **78**, 39–67. Vibrations of three-dimensional pipe systems with acoustic coupling.
6. S. NANAYAKKARA and N. D. PERREIRA 1986 *ASME Journal of Vibration*, *Acoustics*, *Stress*, *and Reliability in Design* **108**, 441–446. Wave propagation and attenuation in piping systems.
7. G. D. C. KUIKEN 1988 *Journal of Fluids and Structures* **2**, 425–435. Amplification of pressure fluctuations due to fluid-structure interaction.
8. M. W. LESMEZ 1989 *Ph.D. Thesis*, *Michigan State University*, *Department of Civil and Environmental Engineering*, *East Lansing*, *USA*. Modal analysis of vibrations in liquid-filled piping systems.
9. M. W. LESMEZ, D. C. WIGGERT and F. J. HATFIELD 1990 *ASME Journal of Fluids Engineering* **112**, 311–318. Modal analysis of vibrations in liquid-filled piping systems.
10. S. C. TENTARELLI 1990 *Ph.D. Thesis*, *Lehigh University*, *Department of Mechanical Engineering*, *Bethlehem*, *USA*. Propagation of noise and vibration in complex hydraulic tubing systems.
11. F. T. BROWN and S. C. TENTARELLI 1988 *Proceedings of the* 43*rd National Conference on Fluid Power*, *USA*, *October*, 139–149. Analysis of noise and vibration in complex tubing systems with fluid–wall interactions.
12. J. CHARLEY and G. CAIGNAERT 1993 *Proceedings of the* 6*th International Meeting of the IAHR Work Group on the Behaviour of Hydraulic Machinery under Steady Oscillatory Conditions*, *Lausanne*, *Switzerland*, *September*. Vibroacoustical analysis of flow in pipes by transfer matrix with fluid–structure interaction.
13. C. A. F. DE JONG 1994 *Ph.D. Thesis*, *Eindhoven University of Technology*, *Eindhoven*, *The Netherlands*, ISBN 90-386-0074-7. Analysis of pulsations and vibrations in fluid-filled pipe systems.
14. C. A. F. DE JONG 1995 *ASME-DE*, 84-2, *Proceedings of the* 1995 *Design Engineering Technical Conferences*, *Boston*, *USA*, *September*, **3**, Part B, 829–834, ISBN 0-7918-1718-0. Analysis of pulsations and vibrations in fluid-filled pipe systems.
15. B. SVINGEN and M. KJELDSEN 1995 *Proceedings of the International Conference on Finite Elements in Fluids—New Trends and Applications*, *Venice*, *Italy*, *October*, 955–963. Fluid structure interaction in piping systems.
16. B. SVINGEN 1996 *Proceedings of the* 7*th International Conference on Pressure Surges and Fluid Transients in Pipelines and Open Channels*, *BHR Group*, *Harrogate*, *UK*, *April*, 385–396. Fluid structure interaction in slender pipes.
17. B. SVINGEN 1996 *Ph.D. Thesis*, *The Norwegian University of Science and Technology*, *Faculty of Mechanical Engineering*, *Trondheim*, *Norway*, ISBN 82-7119-981-1. Fluid structure interaction in piping systems.
18. M. H. CHAUDHRY 1987 *Applied Hydraulic Transients* (second edition). New York: Van Nostrand Reinhold.
19. E. B. WYLIE and V. L. STREETER 1993 *Fluid Transients in Systems*. Englewood Cliffs, New Jersey: Prentice Hall.

20. A. GAJIĆ, S. PEJOVIĆ and Z. STOJANOVIĆ 1996 *Proceedings of the* 18*th IAHR Symposium on Hydraulic Machinery and Cavitation*, *Valencia*, *Spain*, *September*, 845–854, ISBN 0-7923-4210-0. Hydraulic oscillation analysis using the fluid–structure interaction model.
21. T. ADACHI, S. UJIHASHI and H. MATSUMOTO 1991 *ASME Journal of Pressure Vessel Technology* **113**, 517–523. Impulsive responses of a circular cylindrical shell subjected to waterhammer waves.
22. S. GOPALAKRISHNAN, M. MARTIN and J. F. DOYLE 1992 *Journal of Sound and Vibration* **158**, 11–24. A matrix methodology for spectral analysis of wave propagation in multiple connected Timoshenko beams.
23. L. SUO and E. B. WYLIE 1989 *ASME Journal of Fluids Engineering* **111**, 478–483. Impulse response method for frequency-dependent pipeline transients.
24. L. SUO and E. B. WYLIE 1990 *ASCE Journal of Hydraulic Engineering* **116**, 196–210. Hydraulic transients in rock-bored tunnels.
25. L. SUO and E. B. WYLIE 1990 *ASME Journal of Fluids Engineering* **112**, 496–500. Complex wavespeed and hydraulic transients in viscoelastic pipes.
26. T. C. HUANG 1961 *ASME Journal of Applied Mechanics* **28**, 579–584. The effect of rotatory inertia and of shear deformation on the frequency and normal mode equations of uniform beams with simple end conditions.
27. A. E. VARDY, D. FAN and A. S. TIJSSELING 1996 *Journal of Fluids and Structures* **10**, 763–786. Fluid/structure interaction in a T-piece pipe.
28. W. E. BOYCE and R. C. DIPRIMA 1977 *Elementary Differential Equations and Boundary Value Problems* (third edition). New York: John Wiley & Sons.
29. G. G. G. LUESCHEN, L. A. BERGMAN and D. M. MCFARLAND 1996 *Journal of Sound and Vibration* **194**, 93–102. Green's functions for uniform Timoshenko beams.
30. A. E. VARDY and A. T. ALSARRAJ 1991 *Journal of Sound and Vibration* **148**, 25–39. Coupled axial and flexural vibration of 1-D members.
31. R. W. LEONARD and B. BUDIANSKY 1954 *National Advisory Committee for Aeronautics*, *Report* 1173, *Washington*, *USA*. On travelling waves in beams.
32. A. S. TIJSSELING 1993 *Ph.D. Thesis*, *Delft University of Technology*, *Faculty of Civil Engineering*, *Communications on Hydraulic and Geotechnical Engineering*, *Report No.* 93-6, ISSN 0169-6548, *Delft, The Netherlands*. Fluid–structure interaction in case of waterhammer with cavitation.
33. W. FLÜGGE 1942 *Zeitschrift für angewandte Mathematik und Mechanik* **22**, 312–318. Die Ausbreitung von Biegungswellen in Stäben. (The propagation of bending waves in beams.) (in German).
34. L. CREMER, M. HECKL and E. E. UNGAR 1988 *Structure-Borne Sound* (second edition). Berlin: Springer-Verlag.
35. A. E. VARDY and D. FAN 1989 *Proceedings of the* 6*th International Conference on Pressure Surges*, *BHRA*, *Cambridge*, *UK*, *October,* 43–57. Flexural waves in a closed tube.
36. D. C. WIGGERT, R. S. OTWELL and F. J. HATFIELD 1985 *ASME Journal of Fluids Engineering* **107**, 402–406. The effect of elbow restraint on pressure transients.
37. D. C. WIGGERT, F. J. HATFIELD and S. STUCKENBRUCK 1987 *ASME Journal of Fluids Engineering* **109**, 161–165. Analysis of liquid and structural transients by the method of characteristics.
38. D. D. BUDNY, D. C. WIGGERT and F. J. HATFIELD 1991 *ASME Journal of Fluids Engineering* **113**, 424–429. The influence of structural damping on internal pressure during a transient flow.
39. C. S. W. LAVOOIJ and A. S. TIJSSELING 1991 *Journal of Fluids and Structures* **5**, 573–595. Fluid–structure interaction in liquid-filled piping systems.

40. A. S. TIJSSELING, A. E. VARDY and D. FAN 1996 *Journal of Fluids and Structures* **10**, 395–420. Fluid–structure interaction and cavitation in a single-elbow pipe system.
41. G. PAVIĆ 1992 *Journal of Sound and Vibration* **154**, 411–429. Vibroacoustical energy flow through straight pipes.
42. D. FAN 1989 *Ph.D. Thesis*, *The University of Dundee*, *Department of Civil Engineering*, *Dundee*, *UK*. Fluid–structure interactions in internal flows.
43. A. E. VARDY and J. M. B. BROWN 1995 *IAHR Journal of Hydraulic Research* **33**, 435–456. Transient, turbulent, smooth pipe friction.
44. G. E. FORSYTHE and W. R. WASOW 1960 *Finite-Difference Methods for Partial Differential Equations*. New York: John Wiley & Sons.

APPENDIX A: MOC TIME-DOMAIN ANALYSIS

The basic equations (1) are solved in the time domain by the method of characteristics (MOC). A new set of dependent variables is introduced through

$$\boldsymbol{\eta}(z, t) = \mathbf{S}^{-1}\boldsymbol{\phi}(z, t) \quad \text{or} \quad \boldsymbol{\phi}(z, t) = \mathbf{S}\boldsymbol{\eta}(z, t), \tag{A1}$$

so that each η_i is a linear combination of the original variables ϕ_i. Substitution of (A1) into equation (1) gives

$$\mathbf{AS}(\partial/\partial t)\boldsymbol{\eta}(z, t) + \mathbf{BS}(\partial/\partial z)\boldsymbol{\eta}(z, t) = \mathbf{r}(z, t) - \mathbf{CS}\boldsymbol{\eta}(z, t). \tag{A2}$$

Multiplication by $\mathbf{S}^{-1}\mathbf{A}^{-1}$ gives

$$(\partial/\partial t)\boldsymbol{\eta}(z, t) + \boldsymbol{\Lambda}(\partial/\partial z)\boldsymbol{\eta}(z, t) = \boldsymbol{\eta}_{\mathbf{r}}(z, t), \tag{A3}$$

in which

$$\boldsymbol{\Lambda} = \mathbf{S}^{-1}\mathbf{A}^{-1}\mathbf{BS} \tag{A4}$$

and

$$\boldsymbol{\eta}_{\mathbf{r}}(z, t) = \mathbf{S}^{-1}\mathbf{A}^{-1}\{\mathbf{r}(z, t) - \mathbf{CS}\boldsymbol{\eta}(z, t)\}. \tag{A5}$$

A set of equations with a decoupled left side is obtained when $\boldsymbol{\Lambda}$ is a diagonal matrix:

$$\boldsymbol{\Lambda} = \begin{pmatrix} \lambda_1 & 0 & 0 & \cdot \\ 0 & \lambda_2 & 0 & \cdot \\ 0 & 0 & \lambda_3 & \cdot \\ \cdot & \cdot & \cdot & \text{etc.} \end{pmatrix}. \tag{A6}$$

Substitution of equation (A6) into equation (A4) and solving for $\mathbf{S}$ reveals that a non-trivial solution exists only when the diagonal elements of $\boldsymbol{\Lambda}$ are eigenvalues satisfying the *characteristic equation*

$$\det(\mathbf{B} - \lambda\mathbf{A}) = 0, \tag{A7}$$

in which case $\mathbf{S}$ consists of the eigenvectors $\boldsymbol{\xi}_i$ belonging to λ_i:

$$\mathbf{S} = (\xi_1 \quad \xi_2 \quad \cdots \quad \xi_N). \tag{A8}$$

The "decoupled" equations (A3),

$$\partial\eta_i(z, t)/\partial t + \lambda_i \partial\eta_i(z, t)/\partial z = \eta_{ri}(z, t), \quad i = 1, 2, \ldots, N, \tag{A9}$$

transform to

$$\mathrm{d}\eta_i(z, t)/\mathrm{d}t = \eta_{ri}(z, t), \quad i = 1, 2, \ldots, N, \tag{A10}$$

when they are considered along characteristic lines in the z-t plane defined by

$$\mathrm{d}z/\mathrm{d}t = \lambda_i, \quad i = 1, 2, \ldots, N. \tag{A11}$$

The solution of the ordinary differential equations (A10) and (A11) is

$$\eta_i(z, t) = \eta_i(z - \lambda_i \Delta t, t - \Delta t) + \int_{(z-\lambda_i\Delta t,\, t-\Delta t)}^{(z,\, t)} \eta_{ri}(z, t)\, \mathrm{d}t, \quad i = 1, 2, \ldots, N, \tag{A12}$$

when a numerical time step Δt is used, or, with reference to Figure A1,

$$\eta_i(\mathrm{P}) = \eta_i(\mathrm{A}_i) + \int_{\mathrm{A}_i}^{\mathrm{P}} \eta_{ri}(z, t)\, \mathrm{d}t, \quad i = 1, 2, \ldots, N. \tag{A13}$$

Note that, according to definition (A5), η_{ri} depends on η_j ($j = 1, 2, \ldots, N$) if $\mathbf{C} \neq \mathbf{O}$.

The unknown variables η_i at any point P in the interior z-t plane can now be expressed in their values at "earlier" points A_i. A time-marching procedure in combination with a (numerical) integration scheme will give solutions $\boldsymbol{\eta}(\mathrm{P})$ provided that appropriate initial and boundary conditions are given. The original unknowns $\boldsymbol{\phi}$ are obtained from $\boldsymbol{\eta}$ through equation (A1).

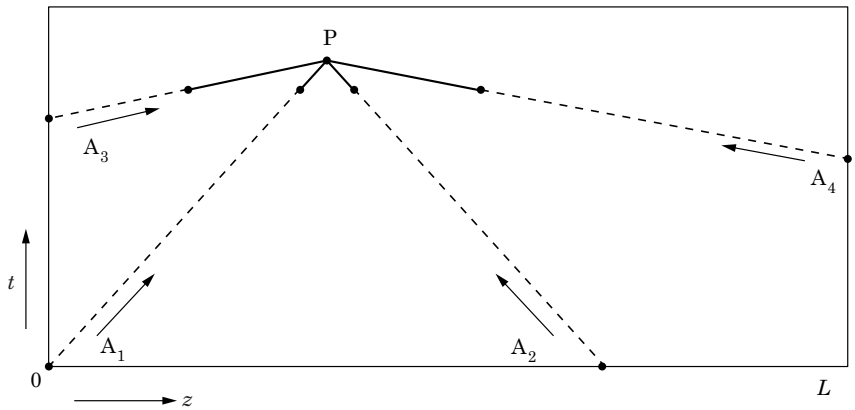

Figure A1. Characteristic lines through point P in the distance-time (z-t) plane. ($N = 4$). Point A_i can be arbitrarily chosen along the characteristic line with slope $1/\lambda_i$.

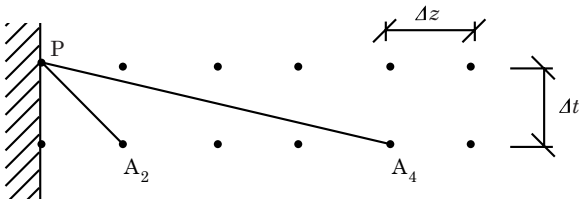

Figure A2. Point P at an end. ($N = 4$).

For the special case that $\boldsymbol{\eta}_\mathbf{r}$ is $\mathbf{0}$, the following analytical solution is derived from equations (A13) and (A1),

$$\boldsymbol{\phi}(\mathrm{P}) = \sum_{i=1}^{N} \mathbf{S}\mathbf{R}_i\mathbf{S}^{-1}\boldsymbol{\phi}(\mathrm{A}_i), \tag{A14}$$

where in the matrix $\mathbf{R}_i$ the ith diagonal element is 1 and all other elements are 0.

Boundary conditions

At the (pipe) ends, the equations (A12) or (A13) provide only $N/2$ relations (see Figure A2). To find the N unknowns $\eta_i(\mathrm{P})$ at the end $z_0 = 0$ (or $z_0 = L$), $N/2$ additional relations are required. These are given by the linear boundary conditions

$$\mathbf{D}(t)\boldsymbol{\phi}(z_0, t) = \mathbf{q}(t) \quad \text{or} \quad \mathbf{D}(t)\mathbf{S}\boldsymbol{\eta}(z_0, t) = \mathbf{q}(t), \tag{A15}$$

where $\mathbf{D}$ is an $N/2 * N$ matrix and the N-vector $\mathbf{q}$ is the boundary excitation.

APPENDIX B: TRANSFORMATION MATRIX S FOR THE FREQUENCY DOMAIN ANALYSIS OF THE LATERAL VIBRATION OF A LIQUID-FILLED PIPE MODELLED AS A TIMOSHENKO BEAM

To maintain the analogy with the MOC analysis in references [44, pp. 38–42] and [32, pp. 97–98], it is helpful to write the transformation matrix $\mathbf{S}$ in the form

$$\mathbf{S}(s) = (\mathbf{T}(s)\mathbf{A}^*(s))^{-1} \quad \text{or} \quad \mathbf{S}(s) = (\mathbf{T}(s)\mathbf{B})^{-1}, \tag{B1}$$

which are two equally valid formulations.

The transformation matrix $\mathbf{T}$ used in the frequency domain analysis herein is given below. With $|s| = \infty$, this matrix is also valid for the MOC time domain analysis presented in Appendix A. The elements of $\mathbf{T}$, derived from

$$\boldsymbol{\Lambda}(s) = \mathbf{T}(s)\mathbf{B}\mathbf{A}^{*-1}(s)\mathbf{T}^{-1}(s), \tag{B2}$$

are

$$t_{11}(s) = 1, \quad t_{12}(s) = \lambda_1(s), \quad t_{21}(s) = t_{11}(s), \quad t_{22}(s) = -t_{12}(s),$$

$$t_{13}(s) = \lambda_1^3(s)s^{-1}/[c_B^2 - \lambda_1^2(s)], \quad t_{14}(s) = (c_B^2/\lambda_1(s))t_{13}(s), \quad t_{23}(s) - t_{13}(s),$$

$$t_{24}(s) = t_{14}(s), \quad t_{31}(s) = \alpha c_B^2 \lambda_3(s)s^{-1}/(\lambda_3^2(s) - c_S^2), \quad t_{32}(s) = \lambda_3(s)t_{31}(s),$$

$$t_{41}(s) = -t_{31}(s), \quad t_{42}(s) = t_{32}(s), \quad t_{33}(s) = 1,$$

$$t_{34}(s) = c_B^2/\lambda_3(s), \quad t_{43}(s) = t_{33}(s), \quad t_{44}(s) = -t_{34}(s), \tag{B3}$$

where $\alpha = \kappa^2 G A_s/EI_s$ and the eigenvalues λ_i are obtained from equation (31).

APPENDIX C: TRANSFORMATION MATRIX **S** FOR THE FREQUENCY DOMAIN ANALYSIS OF THE LONGITUDINAL VIBRATION OF A LIQUID-FILLED PIPE WITH POISSON AND LINEAR FRICTION COUPLING AND WITH VISCOUS STRUCTURAL DAMPING

To maintain the analogy with the MOC analysis in references [44, pp. 38–42] and [32, pp. 78–81], it is helpful to write the transformation matrix **S** in the form (B1).

The transformation matrix **T** used in the frequency domain analysis herein is given below. Without friction and damping effects, that is $f_f = f_s = D_s = 0$, this matrix is also valid for the MOC time domain analysis presented in Appendix A. The elements of **T**, derived from equation (B2), are

$$t_{11}(s) = \left[1 + \frac{2\nu}{\alpha_1(s)}\frac{f_s}{s}\right] \Big/ \left[1 + \frac{f_f}{s} + \frac{1}{\alpha_1(s)}\frac{f_f f_s}{s^2}\right], \quad t_{12}(s) = \lambda_1(s), \quad t_{21}(s) = t_{11}(s),$$

$$t_{22}(s) = -t_{12}(s), \quad t_{13}(s) = \frac{2\nu}{\alpha_1(s)} - \frac{t_{11}(s)}{\alpha_1(s)}\frac{f_f}{s}, \quad t_{14}(s) = [c_s^2/\lambda_1(s)]t_{13}(s),$$

$$t_{23}(s) = t_{13}(s), \quad t_{24}(s) = -t_{14}(s), \quad t_{31}(s) = \rho_f \frac{\nu}{E}\frac{R}{e}\lambda_3^2(s) + \frac{\lambda_3(s)}{c_f^2}t_{32}(s),$$

$$t_{32}(s) = \rho_f \frac{\nu}{E}\frac{R}{e}c_f^2\frac{\lambda_3(s)}{\alpha_3(s)} + \left(\rho_f \frac{\nu}{E}\frac{R}{e}c_f^2\frac{\lambda_3(s)}{\alpha_3(s)}f_f - \frac{c_f^2}{c_s^2}\frac{\lambda_3(s)}{\alpha_3(s)}f_s\right)\frac{1}{s},$$

$$t_{41}(s) = t_{31}(s), \quad t_{42}(s) = -t_{32}(s), \quad t_{33}(s) = \lambda_3^2(s)/c_s^2,$$

$$t_{34}(s) = \lambda_3(s), \quad t_{43}(s) = t_{33}(s), \quad t_{44}(s) = -t_{34}(s), \tag{C1}$$

where

$$\alpha_1(s) = [c_s^2 - \lambda_1^2(s)]/\lambda_1^2(s) - (f_s + D_s)/s, \quad \alpha_3(s) = [c_f^2 - \lambda_3^2(s)]/\lambda_3^2(s) - f_f/s,$$

and the eigenvalues λ_i are obtained from equation (40).

APPENDIX D: NOMENCLATURE

Scalars

A	cross-sectional area, m^2
c	wave speed, m/s
D	damping (per unit length) coefficient, s^{-1}
det	determinant
E	Young modulus of the pipe wall material, Pa
e	pipe wall thickness, m
F	force, N
f	frequency, friction coefficient, s^{-1}
FSI	fluid/structure interaction
G	shear modulus of the pipe wall material, Pa
g	gravitational acceleration, m/s^2
I	second moment of area, m^4
i	imaginary unit
K	fluid bulk modulus, Pa
k	wave number (s/c), m^{-1}
L	length, m
$\mathcal{L}$	Laplace transform
M	bending moment, Nm
m	lumped mass, kg
MOC	method of characteristics
MOC-FFT	method of characteristics followed by fast Fourier transform
mod	modulus
N	number of dependent variables
P	pressure, Pa
Q	shear force, N
R	inner radius of pipe, m
s	Laplace parameter (complex frequency), s^{-1}
T	duration of applied action, s
t	time, s
U	axial velocity, m/s
V	lateral velocity, m/s
z	axial co-ordinate, m
γ	constant, m/s—see equation (41)
Δ	numerical step size
η	loss factor in lateral vibration
κ^2	shear coefficient of the pipe wall material
λ	eigenvalue, m/s
μ	dynamic viscosity, Pas

ν	Poisson ratio
ξ	damping ratio in axial vibration
ρ	mass density, kg/m^3
σ	axial stress, Pa
ψ	rotational velocity of pipe, s^{-1}
Ω	circular frequency of external excitation, rad/s

Matrices and vectors

$\mathbf{A}$	coefficients—see equation (1)
$\mathbf{A}^*$	coefficients—see equation (3)
$\mathbf{B}$	coefficients—see equation (1)
$\mathbf{C}$	coefficients—see equation (1)
$\mathbf{D}$	boundary condition coefficients—see equations (17), (A15)
$\mathbf{D}^*$	modified $\mathbf{D}$—see equation (21)
$\mathbf{E}$	diagonal matrix of exponential coefficients—see equation (15)
$\mathbf{I}$	identity matrix
$\mathbf{M}$	transfer matrix—see equation (27)
$\mathbf{O}$	zero matrix
$\tilde{\mathbf{q}}$, $\mathbf{q}$	boundary condition coefficients (external excitation)—see equations (17), (A15)
$\tilde{\mathbf{q}}^*$	modified $\tilde{\mathbf{q}}$—see equation (23)
$\mathbf{R}$	matrix—see equation (A14)
$\mathbf{r}$	environmental terms—see equation (1)
$\mathbf{S}$	transformation matrix (eigenvectors)—see equations (4), (10), (A1), (A8), (B1)
$\mathbf{T}$	transformation matrix (eigenvectors) in time-domain analysis in references [32] and [44]—see equations (B3), (C1)
$\mathbf{\Lambda}$	diagonal matrix of coefficients (eigenvalues)—see equations (7), (A4), (B2)
$\tilde{\boldsymbol{\eta}}$, $\boldsymbol{\eta}$	composite dependent variables—see equations (4), (A1)
$\tilde{\boldsymbol{\eta}}_\mathbf{r}$, $\boldsymbol{\eta}_\mathbf{r}$	right side in equations (6), (A3)—see equations (8), (A5)
$\tilde{\boldsymbol{\eta}}_\mathbf{r}^*$	particular solution of equation (11)—see equation (13)
$\tilde{\boldsymbol{\eta}}_\mathbf{0}$	constants of integration—see equations (16), (20)
$\boldsymbol{\xi}$	eigenvector—see equation (10)
$\boldsymbol{\phi}$	dependent variables—see equation (1)
$\mathbf{0}$	zero vector

Subscripts

a	air
B	bending (wave speed)
c	cut-on
f	fluid, flow
i	element of vector or matrix
j	element of vector or matrix
L	position $z = L$
n	nth natural frequency
rod	impact rod (in experimental configuration)

S	shear (wave speed)
s	structure, solid
z	axial co-ordinate
0	position $z = 0$

Superscripts

$\sim$	Laplace transformed
T	transposed
-1	inverted